HEAT TRANSFER AND BUBBLE DYNAMICS BEHAVIORS IN SUBCOOLED POOL BOILING AT EARTH GRAVITY AND ISS GRAVITY USING HIGH-FIDELITY CFD SIMULATIONS

Sara Youssoufi[1], Amir Riaz[2], Elias Balaras[1]
[1]George Washington University/Department of Mechanical and Aerospace
Science & Engineering Hall, 800 22nd St NW, Washington, D.C, USA
sarayoussoufi@gwu.edu; balaras@gwu.edu
[2]University of Maryland/Department of Mechanical Engineering
Glenn L. Martin Hall, College Park, MD, USA
ariaz@umd.edu

ABSTRACT

The underlying physics of the effect of subcooling on nucleate boiling remains limited. Overall, subcooled nucleate boiling was assumed to have negligible effects, although it is conjectured that there is a reverse trend in the boiling curve due to subcooling. NASA conducted experiments[1] to investigate the effect of subcooling on both earth-gravity and microgravity conditions. In this work we report interface-resolving, direct numerical simulations that mimic the pool boiling experiments[1] were we consider four subcooling cases in earth-gravity and three subcooling cases in microgravity (ISS). An in-house solver is used to solve the Navier-Stokes equations for incompressible flow, where the working fluid is FC72. The interface between liquid and vapor is tracked using the level set technique. Sharp jumps in pressure, velocity, and temperature are implemented using Ghost Fluid Method. A dynamic contact angle is implemented to consider inertial effects on vapor bubbles due to wall adhesion force. Time advancement is done using a fractional step method where all terms are advanced explicitly using an Adams-Bashforth scheme. Parallelization of the solver is achieved using MPI on distributed memory systems. Our simulations show that subcooling does influence the heat flux trend. The heat flux decreases when the subcooling increases until it reaches an inflection point after which it increases again. Bubble dynamics were studied and coupled to the effect of subcooling on heat flux. The decrease of subcooling before the local minima is due to flow turbulence induced by bubble departure processes, while the increase of heat flux after that is due to bubble coalescence and shrinking at the wall.

NOMENCLATURE, ACRONYMS, ABBREVIATIONS

σ	surface tension of the cooling liquid FC72
δ_{th}	microlayer
h	heat transfer coefficient
q	wall heat flux
$\tilde{q}$	ensemble averaged wall heat flux
$\bar{q}$	time averaged wall heat flux

q' root mean square fluctuations of wall heat flux
$< q'' >$ temporal variation of space averaged wall heat flux
A surface area
P Pressure
T Temperature
Γ interface liquid vapor
κ curvature at the interface liquid vapor
∇T_l heat flux from liquid region
∇T_v heat flux from vapor region
$\vec{\boldsymbol{u}}$ velocity $\vec{u} = (u, v, w)$
u, w velocity components parallel to the heater
v velocity component normal to the heater
u_0 characteristic velocity defined as $u_0 = \sqrt{g l_0}$
l_0 characteristic length scale defined as $l_0 = \sqrt{\sigma/(\rho_l - \rho_v)\, g}$
L_c^g capillary length scale in earth gravity
g earth-gravity $g = 9.8\ m/s^2$
T_{wall} wall/heater temperature
T_{bulk} bulk liquid temperature
T_{sat} saturation temperature of the liquid FC72 ($T_{sat} = 58$°C)
ΔT_{sup} wall superheat defined as $\Delta T_{sup} = T_{wall} - T_{bulk}$
ΔT_{sub} subcooling degree defined as $\Delta T_{sub} = T_{sat} - T_{bulk}$
ρ_l, ρ_v liquid and vapor densities
μ_l, μ_v liquid and vapor thermal viscosities
α_l, α_v liquid and vapor phases
k_l, k_v liquid and vapor thermal conductivities
$\dot{m}$ mass transfer
C_{pl} heat capacity in liquid phase
C_{pv} heat capacity in vapor phase
h_{lv} latent heat of vaporization
St Stefan number $St = C_{pl}\Delta T_{sup}/h_{lv}$
Pr Prandtl number $\mathrm{Pr} = \mu_l C_{pl}/k_l$
Fr Froude number $Fr = u_0/\sqrt{g l_0}$
We Weber number $We = \rho_l u_0^2 l_0/\sigma$
d_{foot} bubble footprint diameter

INTRODUCTION

Thermal systems play an important role in heat transfer management in multiple applications, such as, space, energy, and nuclear reactor industries. These systems face overheating and therefore heat removal techniques are needed. One important heat removal method is pool boiling. The terminology of subcooled pool boiling refers to the state when the bulk liquid temperature (T_{bulk}) is hold at a temperature lower than the saturation temperature of the fluid (T_{sat}). In this work we investigate the effect of subcooled pool boiling first at earth gravity conditions and second at the

international space station (ISS) gravity conditions. We studied the effect on heat transfer, bubble dynamics, and flow statistics. The state of the art concerning pool boiling listed many parameters that would impact the nucleate boiling regime, for example, heater's size[2], material's surface roughness[2], wettability[3], surface tension[4], contact angle[5], boundary layer[6], density of nucleation sites[7], and gravity[1]. This paper will focus on investigating the effect of subcooling and the effect of gravity on nucleate boiling. The goal is to improve the design of cooling systems to achieve better energy efficiency and cost saving design.

Diverse opinions in the literature concerning the effect of subcooling on heat transfer are divided between those who argued about the negligible impact of subcooling and those who emphasize the influence of subcooling on heat flux and bubble dynamics. In the Rhosenow correlation[9], the heat flux coefficient $h = (q/A)/\Delta T_{sup}$ varies as ΔT_{sup}^{3}, where q is the heat flux, A the surface area, and ΔT_{sup} is the superheat temperature defined as the difference between wall temperature and bulk liquid temperature. Other experiments also agree with Rohsenow correlation. Wang and Dhir[3] for example found that $h \sim \Delta T_{sup}^{3}$, Gaertner[10] shows that $h \sim \Delta T_{sup}^{3.75}$, while Son and Dhir[7] and Stephan and Abdelsalam[11] found that $h \sim \Delta T_{sup}$. In addition to these empirical correlations that neglect the effect of subcooling and account only the effect of superheat, we also found Yamagata and Tien[12,13] Zuber and Zuber-Forster[14,15], Forster-Grief[14], and Monde and Katto[16] correlations neglect the effect of subcooling as well. Contrary to the above, several studies have shown that subcooling does influence the heat flux and bubble dynamics. Gunther and Kreith[17] indicate that subcooling prevent bubble from detachment from the heater surface and that vapor departure was replaced by a very tiny hemispherical bubbles of short life cycle that do not detach from the surface. Experimental work of Ibrahim and Judd[18] found that heat flux, bubble growth, and bubble waiting time increase as liquid subcooling increases too, and then up to a critical value of subcooling, beyond which the latest quantities decrease with a further increase in subcooling. This change of trend represents an inflection point situated at 6℃. Goel et al[19] concluded based on experiments that subcooling influences nucleate boiling due to two main effects: first, subcooling enhances the condensation rate at the bubble cap, and second it reduces the evaporation at the bubble base due to the thickness of the superheated liquid layer. Kim and Benton[20], and Kim et al[1] show that subcooling impacts the heat flux due to buoyancy force. Mudawar and Anderson[22] found that subcooling degree influences the critical heat flux and causes a reduction in bubble size. All these empirical heat flux correlations listed above have been studied in subcooled pool boiling context and summarized in the work in reference [23].

Microgravity also affects heat transfer[26, 27, 28, 29]. Previous work shows that the gravity can alter the flow dynamics by dropping the heat transfer[30]. An existing mechanistic model of bubble departure in microgravity was published by Zhao et al[31] where bubble dynamics were divided to four regions with three critical diameter sizes. In these regions, it was observed that tiny bubbles grow until they reach the first critical size to depart, while bigger bubbles with a diameter larger than the second critical size remain attached to the surface and depart only if their diameter exceeds the third critical size.

The present paper aims to highlight the finding of an inflection/minima point when the subcooling increases and study the related bubble dynamics and flow statistics. The identification of this

minima point helps in restricting microgravity studies to most relevant cases and therefore achieve cost-saving high-fidelity computations.

II. METHODOLOGIES AND NUMERICAL SETUP

The present work aims to mimic experiments reported in reference[1]. We consider a pool boiling heat transfer problem over a group of microheater arrays placed inside a boiling chamber. The dynamics of the liquid and the vapor phases are governed by the following equations:

$$\frac{\partial \vec{u}}{\partial t} + \vec{u} \cdot \nabla \vec{u} = -\frac{1}{\rho'} \nabla \mathrm{P} + \nabla \cdot \left[\frac{\mu'}{\rho'} \frac{1}{Re} \nabla \vec{u} \right] + \frac{1}{Fr^2} \tag{1a}$$

$$\frac{\partial \mathrm{T}}{\partial \mathrm{t}} + \vec{u} \cdot \nabla \mathrm{T} = \nabla \cdot \left[\frac{\alpha'}{Re\, Pr} \nabla T \right] \tag{1b}$$

These equations are non-dimensionalized and the relevant non dimensional number for conducted simulations in this research are Reynolds, Prandtl, Froude, and Weber numbers, respectively defined in Equation (2). The in-house solver uses a normalized temperature defined in function of wall temperature and bulk temperature as, $T^* = (T - T_{wall})/(T_{wall} - T_{bulk})$. Each parameter presented in these equations is described in the nomenclature. Note that for the vapor phase: $\rho' = \rho_v/\rho_l$, $\mu' = \mu_v/\mu_l$, and $\alpha' = \alpha_v/\alpha_l$, and for the liquid phase, $\rho' = \mu' = \alpha' = 1$.

$$Re = \rho_l u_0 l_0/\mu_l, \qquad \mathrm{Pr} = \mu_l C_{pl}/k_l, \qquad Fr = u_0/\sqrt{g l_0}, \qquad We = \rho_l u_0^2 l_0/\sigma \tag{2}$$

The equation for conservation of mass can be written as in Equation (3), where $\vec{n}$ is a unit vector normal to the interface, and $\dot{m}$ is the mass transfer calculated using Equation (4). St is the Stefan number defined as $St = C_{pl}\Delta T/h_{lv}$:

$$\nabla \cdot \vec{u} = -\dot{m} \nabla \frac{1}{\rho'}|_\Gamma \cdot \vec{n} \tag{3}$$

$$\dot{m} = \frac{St}{Re\, Pr} [\nabla T_l|_\Gamma \cdot \vec{n} - k' \nabla T_v|_\Gamma \cdot \vec{n}] \tag{4}$$

Note that ∇T_l is the heat flux from the liquid region that contributes towards evaporation, and ∇T_v is the heat flux from vapor region that accounts for condensation.

The system of equations described above is solved using a DNS in-house solver. The latter is based on a single-fluid with variable properties approach, and a level set method to track the interface Γ between liquid and vapor phases. A cartesian grid with a staggered arrangement of the flow variables is adopted. Finite difference methods are used to approximate all spatial derivatives. Time advancement is achieved using a fractional step method where all terms are advanced explicitly using an Adams-Bashforth scheme. Ghost Fluid Method (GFM) is used to enforce boundary conditions for the velocity, pressure and temperature at the liquid-vapor phase interface Γ, details on the considered GFM method are outlined in reference[24].

$$[P]_\Gamma = P_v - P_l = \frac{\kappa}{We} - \left(\frac{1}{\rho'} - 1\right)\dot{m}^2 \tag{5a}$$

$$[\vec{u}]_\Gamma = \vec{u}_v - \vec{u}_l = \dot{m}\left(\frac{1}{\rho'} - 1\right)\vec{n} \tag{5b}$$

$$T_\Gamma = T_{sat} \tag{5c}$$

Details on solver implementations of the above equations with an extensive validation of pool boiling problems can be found in reference [25].

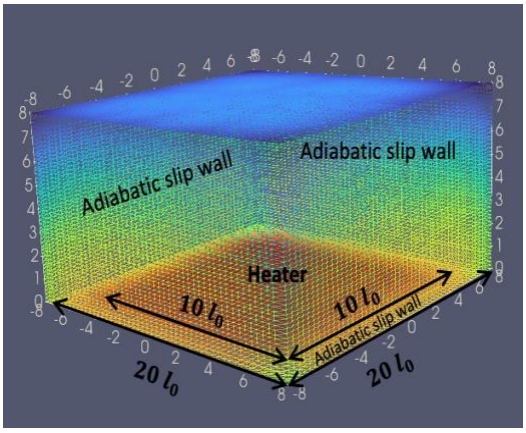

Figure 1: Computational domain for subcooled pool boiling problem

The computational domain, designed to mimic experiments reported in reference[1], is presented in Figure 1. A group of micro-heaters of 96 platinum resistance heaters in 10×10 configuration arrangement is placed inside a boiling chamber. The size of each heater is $0.7\ mm \times 0.7\ mm$ resulting in $7\ mm \times 7\ mm$ as a total heated area. The size of the boiling chamber is $288\ mm \times 144\ mm \times 144\ mm$. In Figure 1, all lengths are normalized by the reference length scale $l_0 = 0.7\ mm$, corresponding to the capillary length L_c^g in earth gravity, $g = 9.8\ m/s^2$.

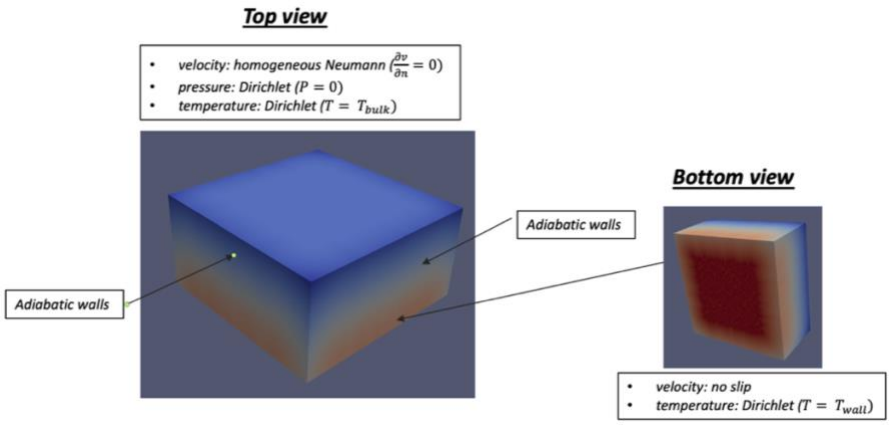

Figure 2: Applied boundary conditions considered in pool boiling DNS simulations

Regarding the applied boundary conditions, on the wall heated area, a no-slip boundary condition is enforced for the velocity field and a Dirichlet boundary condition is considered for the temperature ($T = T_{wall}$). At the top of the computational domain, homogeneous Neumann boundary condition ($\partial v/\partial n = 0$) is applied to the velocity, while Dirichlet boundary conditions are used for the pressure ($P = 0$) and temperature ($T = T_{bulk}$). The remaining portions of the computational domain along the sides are modelled as adiabatic slip walls. Figure 2 illustrates the boundary conditions considered in this study. The working fluid in all cases is FC-72 where the values of physical parameters are listed in Table 1.

σ	h_{lv}	ρ_l	ρ_v	μ_l	μ_v	k_l	k_v	C_{pl}	C_{pv}
$8.3e^{-3}$	83562	1620	13.5	$4e^{-4}$	$4e^{-4}$	$5.4e^{-2}$	$1.35e^{-2}$	1110	925
N/m	J/kg	kg/m^3	kg/m^3	Ns/m^2	Ns/m^2	W/mK	W/mK	K/kgK	K/kgK

Table 1: Physical properties of the refrigerant FC 72

Fundamental physics of nucleate boiling is illustrated in Figure 3. A bubble life cycle starts with bringing the coolest liquid near the wall; as a result, a rapid cooling occurs during nucleation and growth stages. Once the bubble detaches from the wall, the temperature of the cold spot increases. A group of cold spots heated up and form a microlayer (δ_{th}). Once the microlayer is heated enough, new bubbles are formed, they grow and detach from the surface.

In the present paper we conducted 5 subcooled pool boiling computations at earth gravity conditions (case 1E, case 2E, case 3E, case 4E, and case 5E), and 3 subcooled pool boiling conditions at microgravity corresponding to the international space station (ISS) gravity (case 1ISS, case 2ISS, case 3ISS). Cases from 1E to 5E are presented to highlight a general overview on the effect of subcooling on heat flux. Later in this paper, we will focus on cases 1E, 1ISS, 2E, 2ISS, 3E, 3ISS.

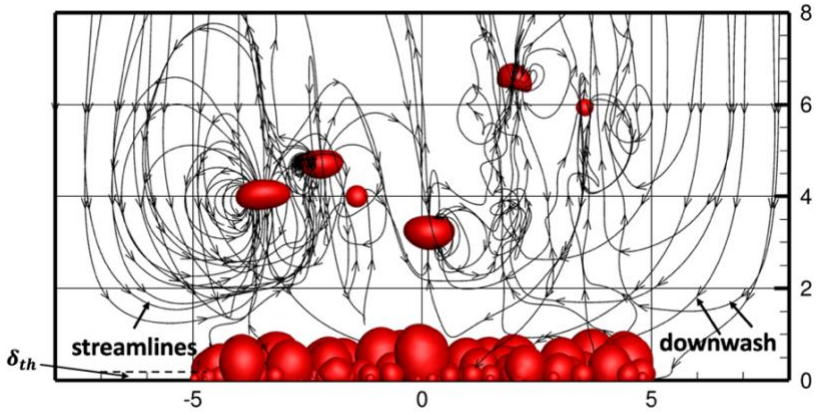

Figure 3: Fundamental mechanisms of pool boiling

For all cases, the temperature of the heater is maintained constant at $T_{wall} = 92$℃, the saturation temperature of the refrigerant is set at $T_{sat} = 58$ ℃, therefore the superheat degree $(\Delta T_{sup} = T_{wall} - T_{sat})$ is maintained constant at 34℃ for all cases. The bulk liquid temperature

of the refrigerant is varied to capture different level of subcooling degree from low subcooling ($\Delta T_{sub} = 5℃$) to high subcooling ($\Delta T_{sub} = 25℃$) at earth gravity and focuses on three subcooled cases at ISS gravity ($\Delta T_{sub} = 8℃,\ 11℃,\ 13℃$). Parameters considered in the DNS simulations for all the studied cases are summarized in Table 2. The difference between cases named E and cases named ISS is the gravity (in dimensionless unit $g = 1$ for earth gravity while $g = 10^{-4}$ for ISS gravity). Note that St^* in Table 2 corresponds to the dimensionless Stefan number.

Cases	$T_{bulk}(℃)$	$T_{wall}(℃)$	$\Delta T_{sub}(℃)$	St^*
1E, 1ISS	50	92	8	0.5579
2E, 2ISS	47	92	11	0.5978
3E, 3ISS	45	92	13	0.6243
4E	40	92	18	0.6907
5E	33	92	25	0.7837

Table 2: Description of the computational cases

Note that the present work does not resolve the effect of the surface roughness as we consider a smooth wall. To focus on the effect of subcooling and the gravity, the nucleation sites are considered constant as they are extracted from an experimental correlation relating the nucleation sites to the wall superheat[21]. The distribution of quasi-random nucleation sites density was obtained using a Monte Carlo discrepancy algorithm. The later introduces a bubble embryos diameter of a 2 – 3 local grid cells. The growth of the bubble embryos is obtained by evaporation process. For the considered wall superheat $\Delta T_{sup} = 34℃$, nucleation bubble density is estimated to 6 $bubbles/mm^2$, which corresponds to 600 bubbles in a total.

III. RESULTS

High fidelity CFD-DNS computations have been conducted to mimic experiments reported in reference[1]. A qualitative comparison is shown in Figure 4. At earth gravity, we have the formation of multiples bubbles that grow, merge, and depart, while at microgravity we have the formation of big bubble surrounded by tiny bubbles. Figure 4 shows that DNS simulations match results obtained from NASA experiments[1]. Note that CFD-DNS results in Figure 4(b) corresponds to a case of saturated pool boiling. For subcooled pool boiling in ISS gravity, instead of having one big bubble, we obtained multiple big bubbles as can be seen from Figure 5.

Figure 6 shows the temporal variation of space averaged wall heat flux $< q'' > (W/cm^2)$ at earth gravity (Figure 6.a) and ISS gravity (Figure 6.b). Since the solver is dimensionless, dimensional heat flux q'' was obtained from dimensionless heat flux q''^* using Equation (6). Note that cases from 0E to 5E and cases from 1ISS to 3ISS as well as saturated cases were all conducted using the same initial conditions. Only bulk liquid temperature and gravity are varied.

$$q'' = k_l \frac{T_{wall} - T_{liq}}{l_0} q''^* \tag{6}$$

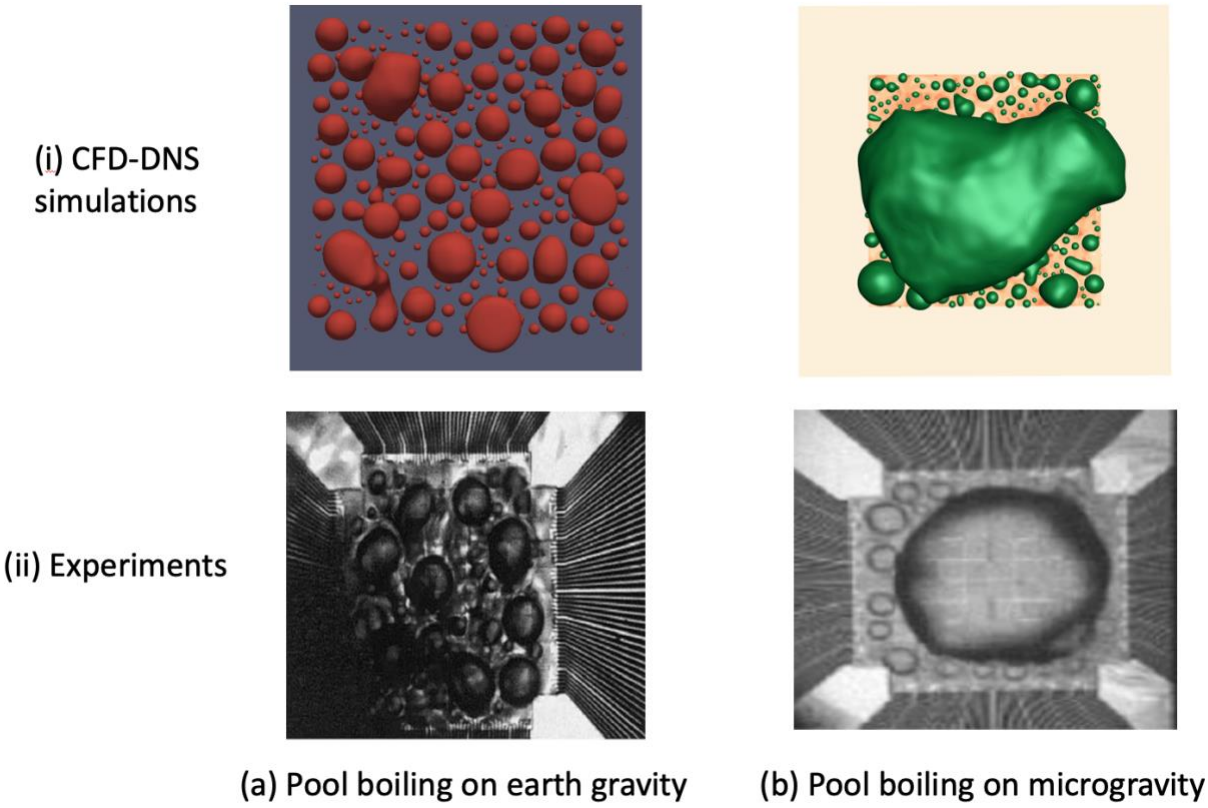

Figure 4: Overview comparison of bubble dynamics at earth gravity and microgravity between parabolic flight experiments[1] and our CFD DNS computations

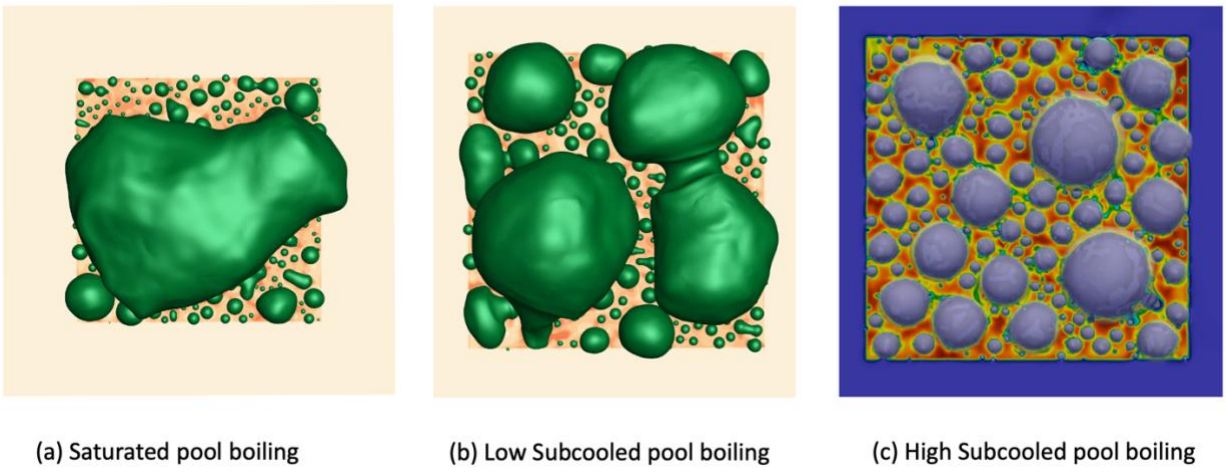

Figure 5: CFD DNS at ISS gravity: (a) Saturated pool boiling (b) low subcooled pool boiling (c) high subcooled pool boiling

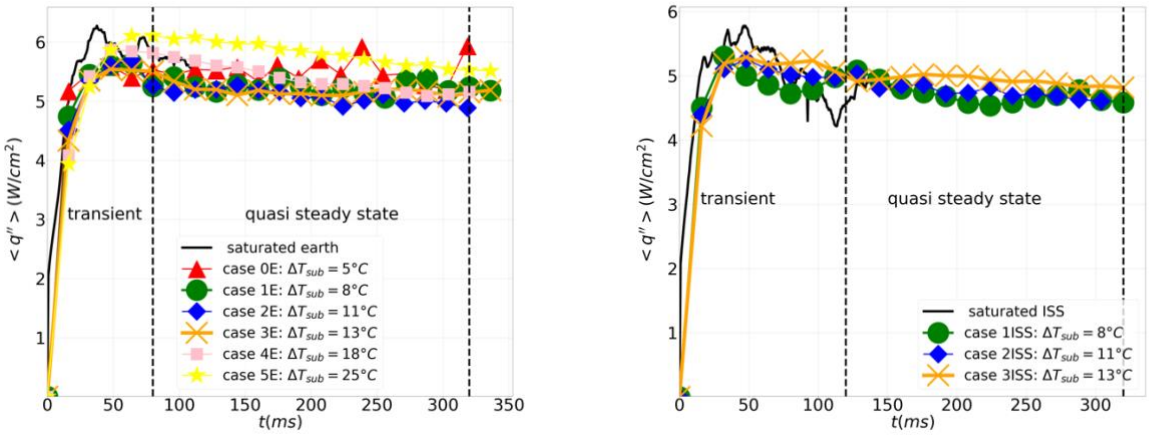

(a): Earth gravity (b): ISS gravity

Figure 6: Temporal variation of the dimensional space averaged wall heat flux $< q'' >$ (W/cm^2) for different subcooled pool boiling cases: (a): at earth gravity, (b): at International Space Station (ISS) gravity.

It can be observed from Figure 6.a that the heat flux decreases with increasing the subcooling degree from case 0E to case 2E. After reaching subcooling degree $\Delta T_{sub} = 11$℃ (case 2E), we observe that the heat flux increases in cases 3E, 4E, and 5E. Same observations are noticed at ISS gravity, as can be seen from Figure 6.b, the space averaged wall heat flux $< q'' >$ is decreasing in case 1ISS and case 2ISS, while $< q'' >$ in case 3ISS is clearly increasing above cases 1ISS and 2ISS. These observations are clearly highlighted by tracking the evolution of the ensemble averaged wall heat flux $\tilde{q}$ (W/cm^2) as a function of subcooling temperature degree, calculated using Equation (7) as:

$$\tilde{q} = \frac{\sum_{n_i}^{N_z} \sum_{n_i}^{N_x} \sum_{n_i}^{N_{samples}} q}{\sum_{n_i}^{N_z} \sum_{n_i}^{N_x} \sum_{n_i}^{N_{samples}}} \quad (7)$$

Where n_i corresponds to the time when the quasi-steady state regime is reached and $N_{samples}$ corresponds to the total number of statistically independent snapshots in the quasi-steady state regime. A total of $N_{samples} = 40$ is considered in this study. Note that N_x and N_z in Equation (7) correspond to the computational points respectively in x and z directions. Plot result is shown in Figure 7. We conclude that subcooled pool boiling influences the heat flux on both earth gravity and ISS gravity. Using FC72 as a cooling refrigerant, the heat flux decreases when the subcooling degree increases until $\boldsymbol{\Delta T_{sub} = 11}$℃, beyond this value, heat flux shows a reverse trend. This result agrees with the work of Ibrahim and Judd (1985)[18] who highlight similar trend for the heat flux in function of subcooling degree and observe the existence of an inflection point situated at $\boldsymbol{\Delta T_{sub} = 6}$℃. In our cases, for subcooled nucleate boiling using FC72 as a working fluid refrigerant, the inflection/minima point is situated at $\boldsymbol{\Delta T_{sub} = 11}$℃ at both earth and ISS gravities.

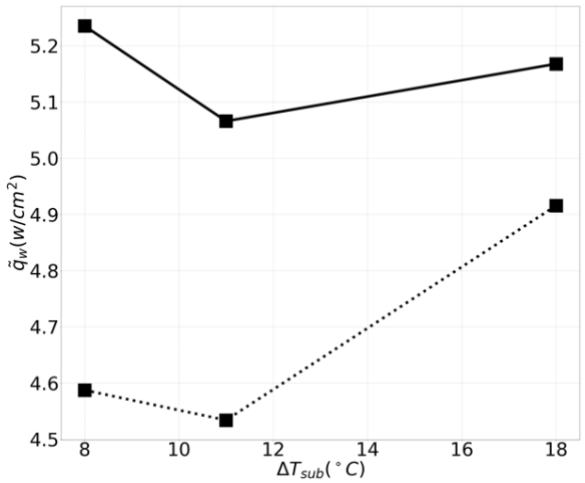

Figure 7: Ensemble averaged wall heat flux as a function of subcooling temperature at both earth gravity (solid line ___) and ISS gravity (dash line ….)

Figure 8 highlights a comparison for same subcooled degrees at earth and ISS gravity. It can be observed that at ISS gravity longer time is needed to reach the steady state period than at earth gravity. Steady state period starts at 80 ms at earth gravity while it starts at 120 ms at ISS gravity. Moreover, in the steady state regime, we observe that the mean of $< q'' >$ decreases by 4.58% in low subcooling between earth gravity (case 1E) and ISS gravity (case 1ISS), and by 4.06% in high subcooling between earth gravity (case 3E) and ISS gravity (case 3ISS). Clearly the effect of gravity on heat flux is stronger in low subcooling than in high subcooling.

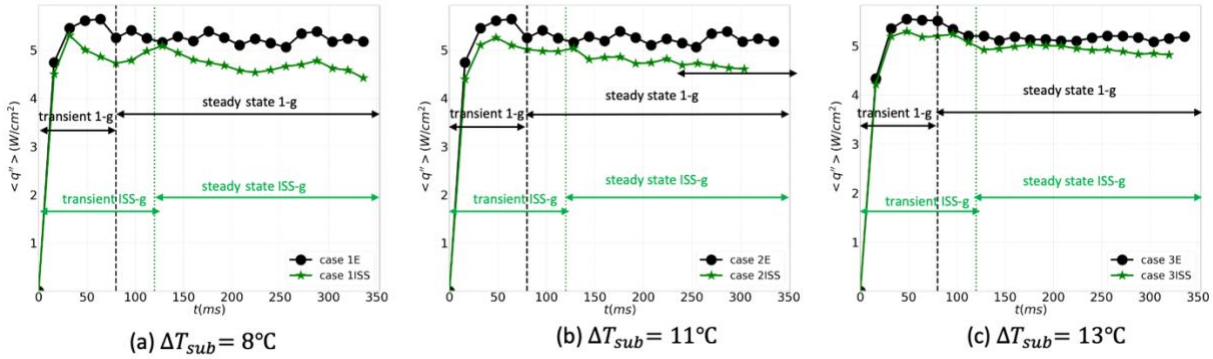

Figure 8: Comparison of temporal variation of space averaged wall heat flux between earth gravity (1-g) and ISS gravity (ISS-g) for (a) low subcooling, (b) intermediate subcooling, and (c) high subcooling

To get a clear understanding of the heat flux trend, we computed time averaged wall heat $\bar{q}\ (W/cm^2)$ and its root mean square fluctuation $q'\ (W/cm^2)$ in the steady state regime as follow:

$$\bar{q} = \frac{\sum_{n_i}^{N_{samples}} q}{\sum_{n_i}^{N_{samples}}} \tag{8}$$

$$q' = \sqrt{\frac{\sum_{n=1}^{N_z} \sum_{n=1}^{N_x} \sum_{n_i}^{N_{samples}} (q - \tilde{q})^2}{\sum_{n=1}^{N_z} \sum_{n=1}^{N_x} \sum_{n_i}^{N_{samples}}}} \tag{9}$$

From Figure 9, Figure 10, Figure 11, and Figure 12 we observe that high subcooled pool boiling ($\Delta T_{sub} = 13℃$) shows more dry spots than low subcooled pool boiling ($\Delta T_{sub} = 8℃$) at both earth gravity and ISS gravity. We also observe that the root mean square fluctuations of wall heat flux q' at both 1-g and ISS-g is higher in high subcooled pool boiling ($\Delta T_{sub} = 13℃$) compared to low subcooled pool boiling ($\Delta T_{sub} = 8℃$). This indicates that the degree of subcooled pool boiling has an impact on the vapor dry spot dynamics at both earth and ISS gravity conditions. We also observe that, at the same degree of subcooling temperature, the gravity influences the size of the dry spots. Tiny bubbles are observed at both earth gravity and microgravity at all degrees of subcooling temperature, while big bubbles are observed only in ISS gravity. These observations agree with the work of Zhao et al [21].

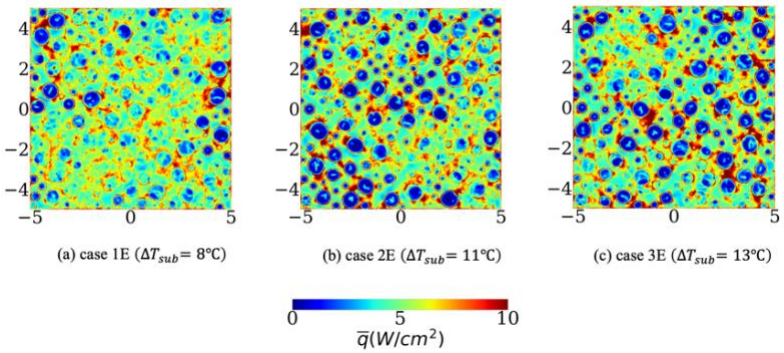

Figure 9: Time-averaged overall wall heat flux $\bar{q}(W/cm^2)$ at earth gravity

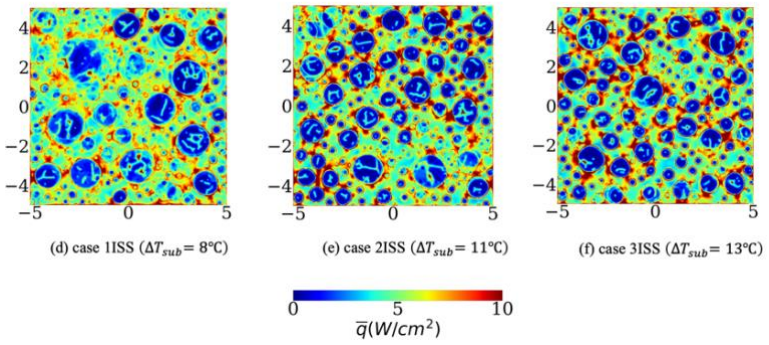

Figure 10: Time-averaged overall wall heat flux $\bar{q}(W/cm^2)$ at ISS gravity

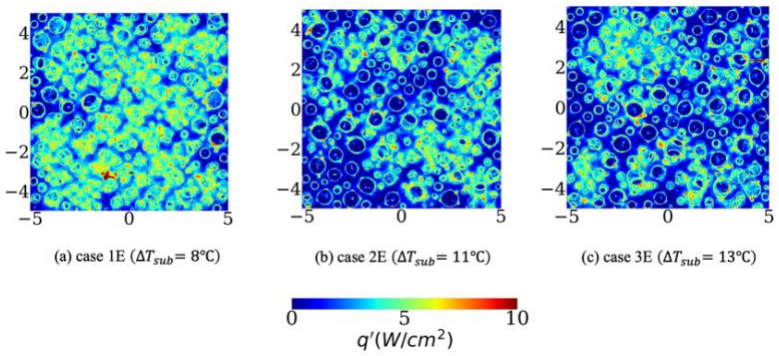

Figure 11: rms fluctuations of overall wall heat flux $q'(W/cm^2)$ at earth gravity

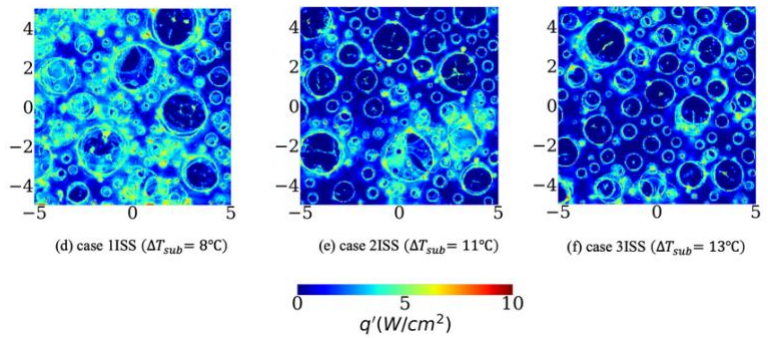

Figure 12: rms fluctuations of overall wall heat flux $q'(W/cm^2)$ at ISS gravity

Next, we developed a tracking algorithm that captures attached and detached bubbles and provides bubble properties such as centroid coordinates, bubble diameters, area, and volume. In summary, the developed algorithm uses scikit library[8] and consists of the following steps:

1. Define the interface from the level set function (ϕ)
2. Apply thresholding to tag each bubble using the level set function $(bubble = \phi \geq 0)$
3. Apply the connectivity to tag each bubble with a unique region
4. Measure the bubble properties. Bubble properties are obtained in pixel unit, interpolation is needed to convert bubble properties to the solver units.

We used this algorithm to track bubbles attached to the surface of the heater by taking a slice in y direction equal to the grid size $(y = 0.033)$ and we constructed the probability density function (PDF) of the statistical distribution of attached bubble diameter, we named the diameter of the attached bubbles footprint diameter d_{foot}. Figure 13 shows the PDF results obtained at earth gravity for low subcooling case 1E $(\Delta T_{sub} = 8℃)$, and high subcooling case 3E $(\Delta T_{sub} = 13℃)$, while Figure 14 presents the PDF of footprint diameters at ISS gravity for low subcooling case 1ISS $(\Delta T_{sub} = 8℃)$, and high subcooling case 3ISS $(\Delta T_{sub} = 13℃)$.
Note that PDF are computed from data in the steady state regime.

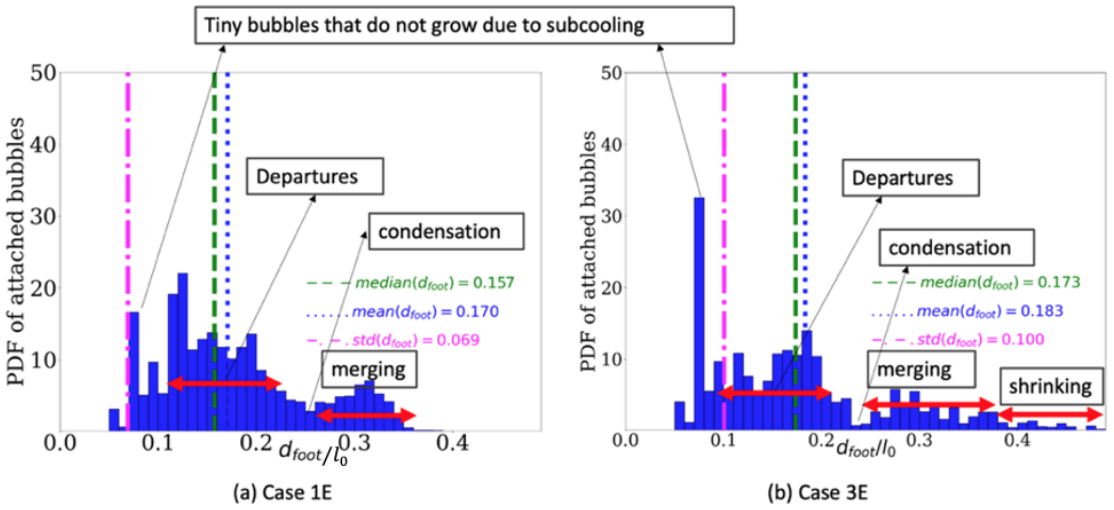

Figure 13: PDF of footprint diameters of attached bubbles at earth gravity for (a): low subcooling case 1E ($\Delta T_{sub} = 8$℃) , and (b): high subcooling case 3E ($\Delta T_{sub} = 13$℃).

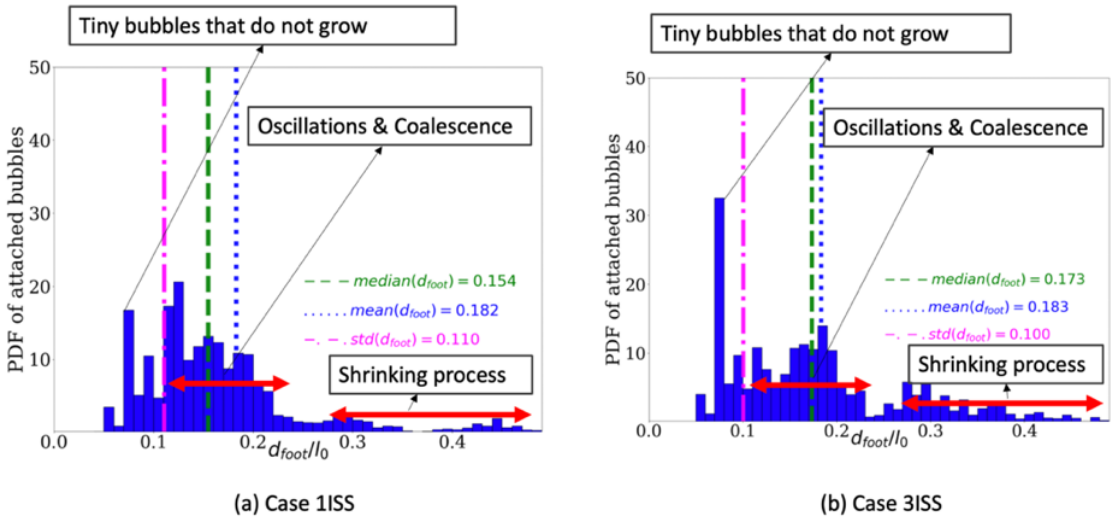

Figure 14: PDF of footprint diameters of attached bubbles at ISS gravity (a): low subcooling case 1ISS ($\Delta T_{sub} = 8$℃), and (b): high subcooling case 3ISS ($\Delta T_{sub} = 13$℃)

By relating these PDF statistical distribution results to the qualitative dynamic of the bubbles in flow visualizations, we observed that the dynamics at earth gravity is governed by bubble departures, condensation and merging processes for both low and high subcooling, while shrinking of bubbles was observed only at high subcooling. Figure 15 highlights these findings. In the meanwhile, at ISS gravity, bubble dynamics was observed to be governed by lateral bubble coalescences leading to big bubbles at both low and high subcooling, as illustrated in Figure 16.

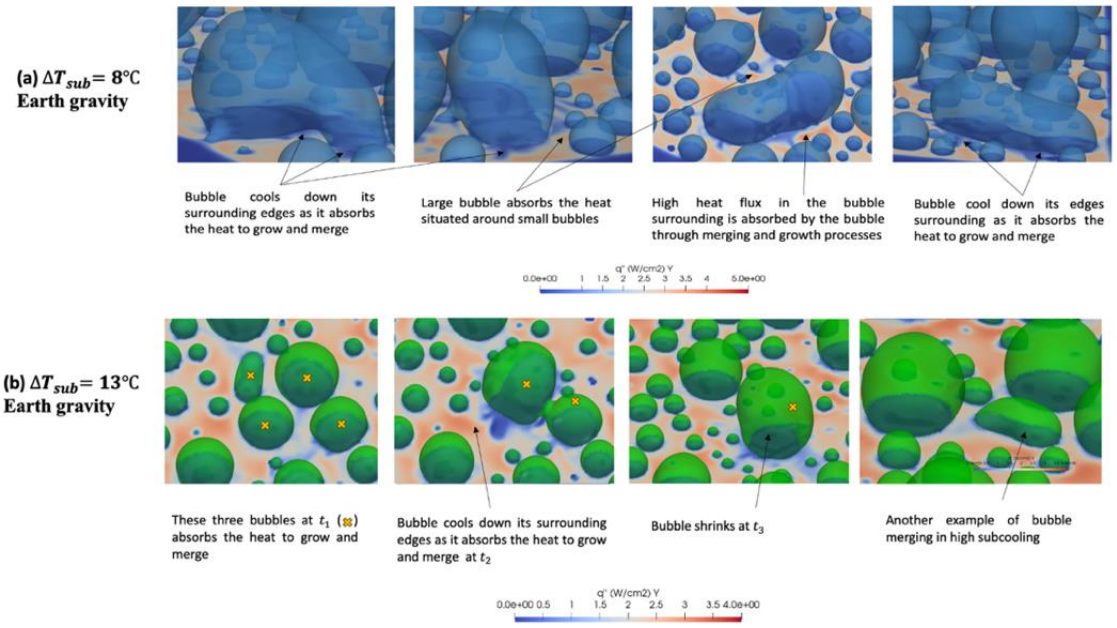

Figure 15: Earth gravity bubble dynamics (a) low subcooling case 1E highlighting growth and merging processes, (b) high subcooling case 3E highlighting growth, merging, and shrinking processes.

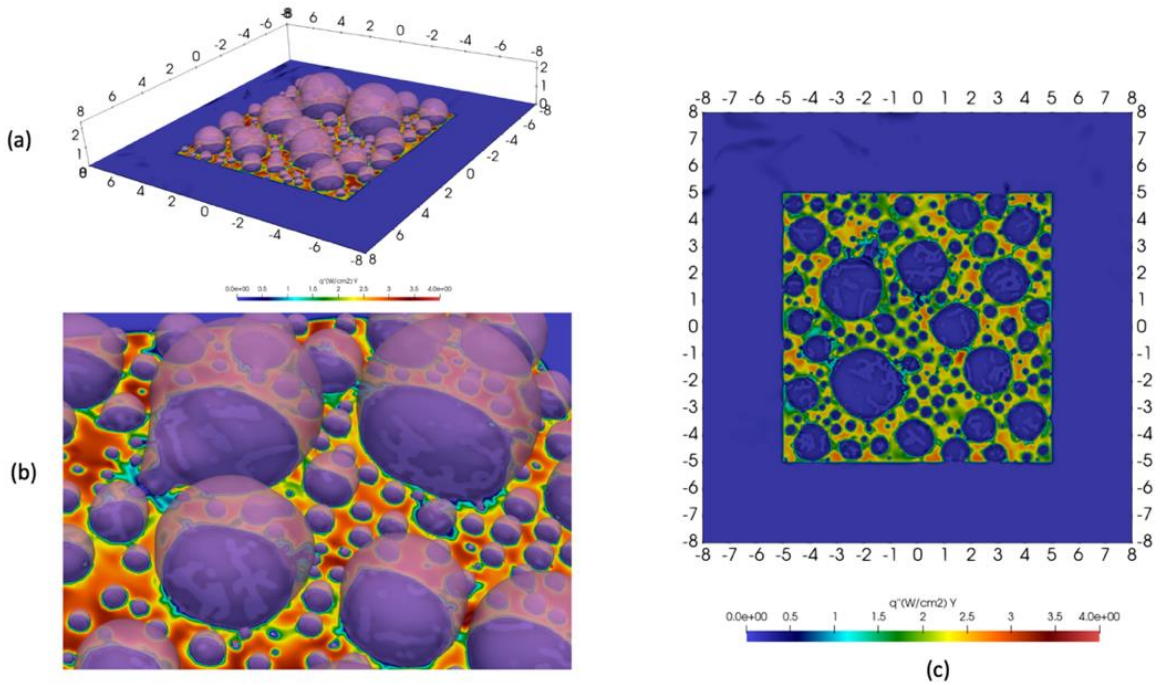

Figure 16: ISS gravity bubble dynamics in low subcooling ($\Delta T_{sub} = 8℃$) at t = 328 ms highlighting the growth big bubbles by merging with the surrounding tiny bubbles (a): 3D view, (b): zoom on the 3D view, (c): bottom view

Bubble shrinking, illustrated in Figure 17, was observed to be only a quality of high subcooled boiling at earth gravity, while at ISS-gravity, the shrinking was observed at both low and high subcooling with the highest presence in high subcooling (case 3ISS). This could explain why for high subcooling the difference between the heat flux at earth gravity and the heat flux at ISS gravity is smaller (4.06%) than this difference observed in low subcooling (4.58%) (Figure 8). Therefore, bubble shrinking process could be a key element influencing the difference in heat flux trend between ISS and earth gravities.

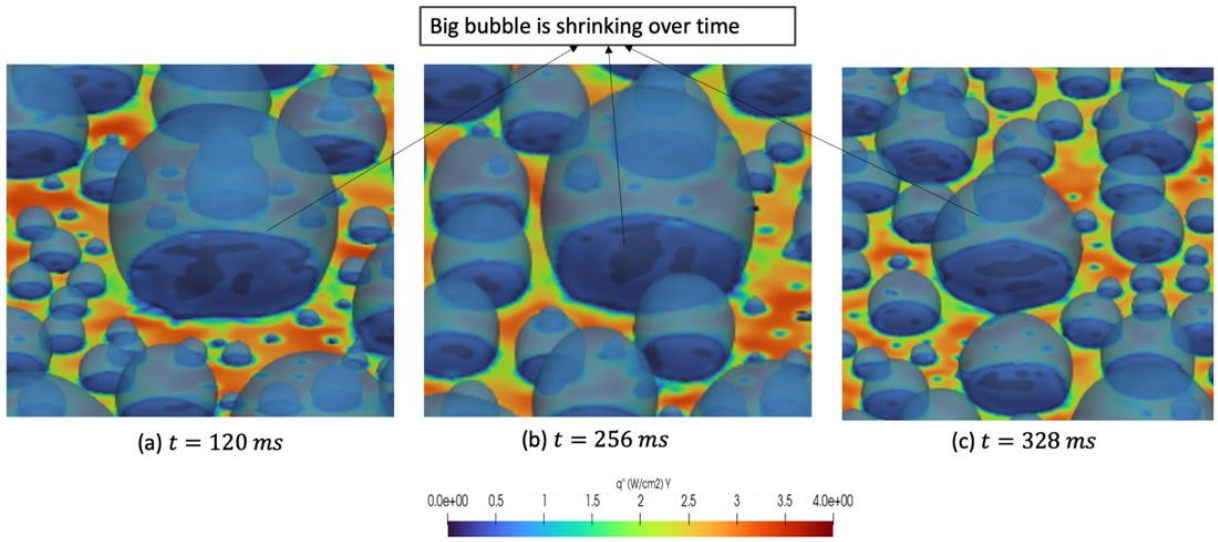

Figure 17: ISS gravity bubble dynamics in high subcooling ($\Delta T_{sub} = 13$℃) at different time highlighting shrinking of big bubble and growth of tiny bubbles

Next, regarding bubble departure processes, it was observed that bubble departure population decreases when increasing the subcooling temperature. As the subcooling increases, less heat is provided to the bubbles which reduce their abilities to grow, therefore the minimal diameter required for departure is hardly reached, leading to a decrease in bubble departure frequencies. Figure 18 highlights these observations at earth gravity. Using the same developed algorithm described before, we tracked the departed bubbles from the time of their detachment until they reach the artificial condensation area situated at $y/l_0 = 6$. The mean equivalent departure diameter is 0.96 mm for case 1E, 0.77 mm for case 2E, and 0.67 mm for case 3E.

At ISS gravity, no departures were observed for cases 2ISS, and 3ISS, a very few negligible departed bubbles were observed for case 1ISS as illustrated in Figure 19. Regarding the existing literature, a mechanistic model of bubble departures in microgravity, including ISS gravity, was developed by Zhao et al[31]. This model describes the dynamic of the bubble in function of the bubble diameter. Bubble attachment was related to regions when $D_{bubble} \leq 0.13\ mm/l_0$ and $3.4\ mm/l_0 \leq D_{bubble} \leq 8.6\ mm/l_0$, while bubble departures were attributed to regions when $0.13\ mm/l_0 \leq D_{bubble} \leq 3.4\ mm/l_0$ and $D_{bubble} \geq 8.6\ mm/l_0$. Following this model, we should observe in our cases bubble attachment when $d_{foot}/l_0 \leq 0.18$ and bubble departures when $0.18 \leq d_{foot}/l_0 \leq 4.8$. However, as seen in Figure 13 and Figure 14 and validated by qualitative visualizations (Figure 16 and Figure 17), only attachment process follows the model above. The

differences between our findings and Zhao et al[31] model could be due to the type of refrigerant and the effect of subcooling.

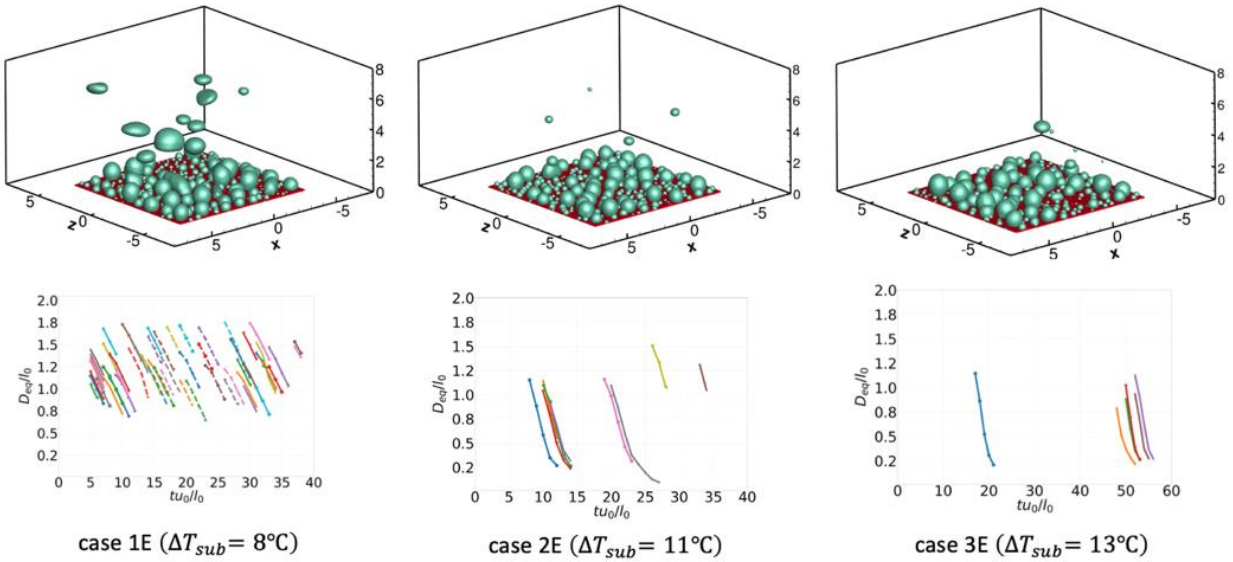

Figure 18: Earth gravity bubble departures at different subcooling degree.

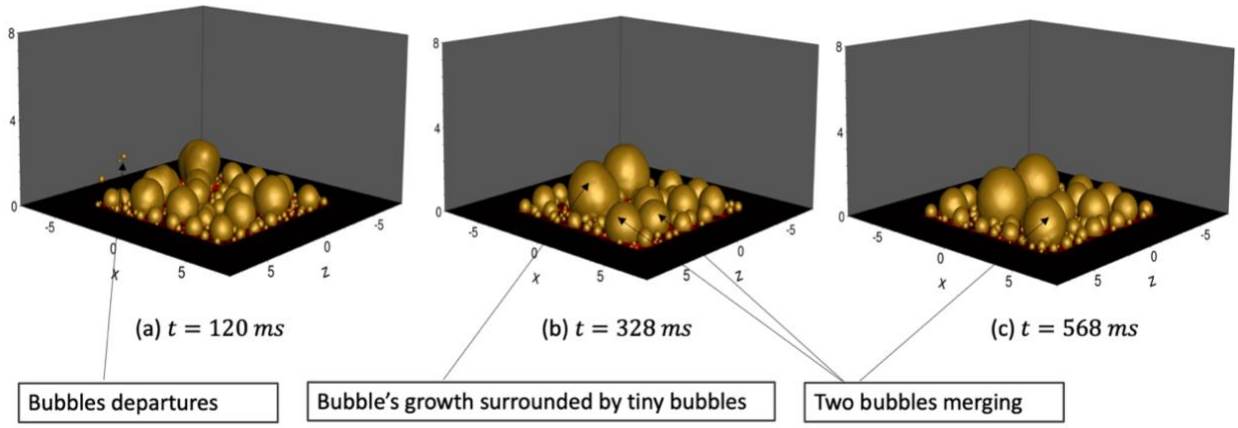

Figure 19: ISS gravity bubble dynamics in low subcooling ($\Delta T_{sub} = 8$°C) highlighting departure, growth, and merging processes.

To understand clearly the dynamics described in PDF (Figure 13 and Figure 14) and the associated qualitative observations (Figure 15, Figure 16, Figure 17), we computed the rms fluctuations of temperature as illustrated in Figure 20, Figure 21. At near wall interactions ($y/l_0 = 1$), all subcooled cases at earth gravity decreases at the same point ($T' = 0.09$) while at ISS gravity a small difference in temperature fluctuations between low and high subcooling is observed. Clearly rms temperature in ISS gravity is affected by bubbles shrinking process. Further away from the wall ($y/l_0 > 1$), we observe a rapid decrease in the rms temperature at ISS gravity compared to

earth gravity . This could be explained by the total absence of bubble departure in ISS gravity and its higher bubbles growth ratio compared to earth gravity.

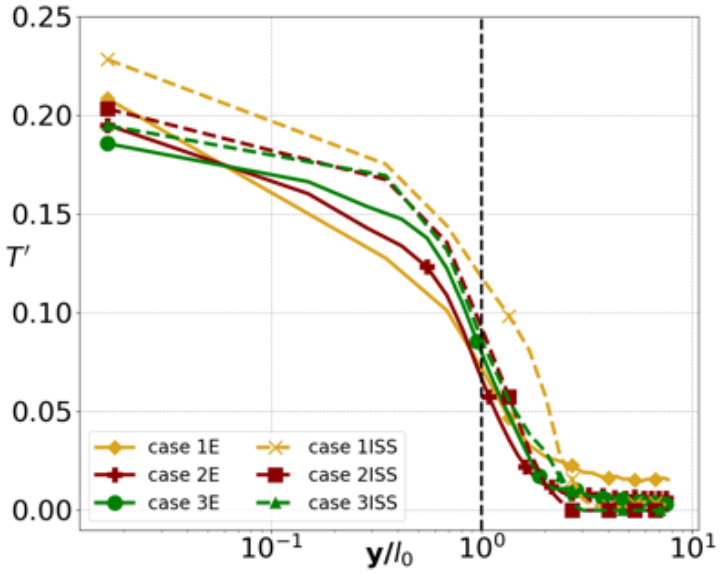

Figure 20: rms temperature fluctuations at earth and ISS gravities for all cases

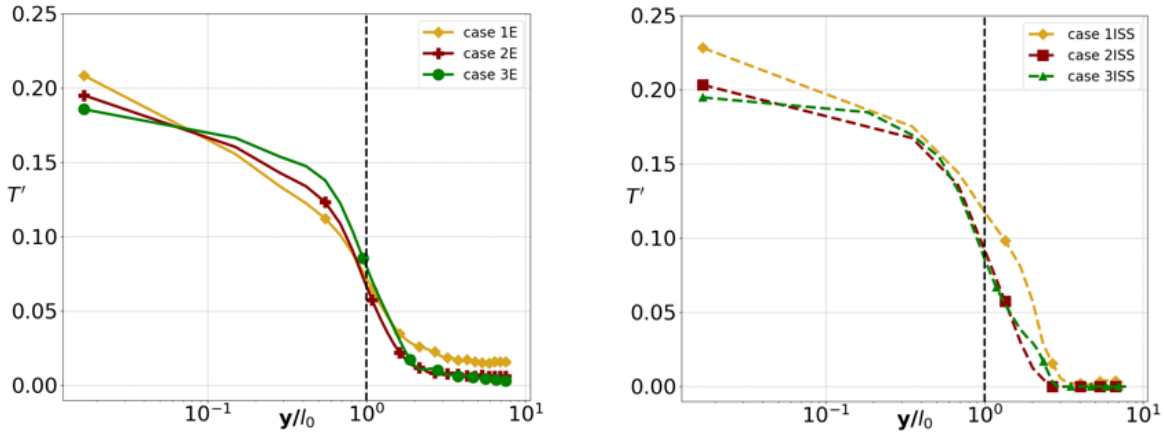

Figure 21: rms temperature fluctuations at earth and ISS gravities for all cases

Regarding the rms velocity fluctuations, all components $\boldsymbol{u}'$, $\boldsymbol{v}'$, and $\boldsymbol{w}'$ were computed and plotted in Figure 22, and Figure 23. Note that $\boldsymbol{u}'$ and $\boldsymbol{w}'$ are velocity components parallel to the heater and $\boldsymbol{v}'$ is the normal velocity component. At near wall, we observe that $\boldsymbol{v}'$is smaller than the horizontal components $\boldsymbol{u}'$and $\boldsymbol{w}'$. Further away from the wall, we observe higher fluctuations in $\boldsymbol{u}'$ and $\boldsymbol{w}'$ in ISS gravity compared to earth gravity. This is caused because bubbles in ISS gravity are bigger and behave as a sink bubble that absorb all tiny bubbles situated around. Further away from the wall, vertical component ($\boldsymbol{v}'$) show more oscillations at earth gravity compared to ISS gravity, this is due to departure processes. While at near wall interactions, we observe a significant difference

in terms of v' between ISS and earth gravity due to the growth ratio process that is bigger at ISS compared to earth gravity. We also observe that differences between ISS and earth gravity tend to be reduced when subcooling increases. Therefore, flow statistics for high subcooled cases at ISS gravity is like the one at earth gravity.

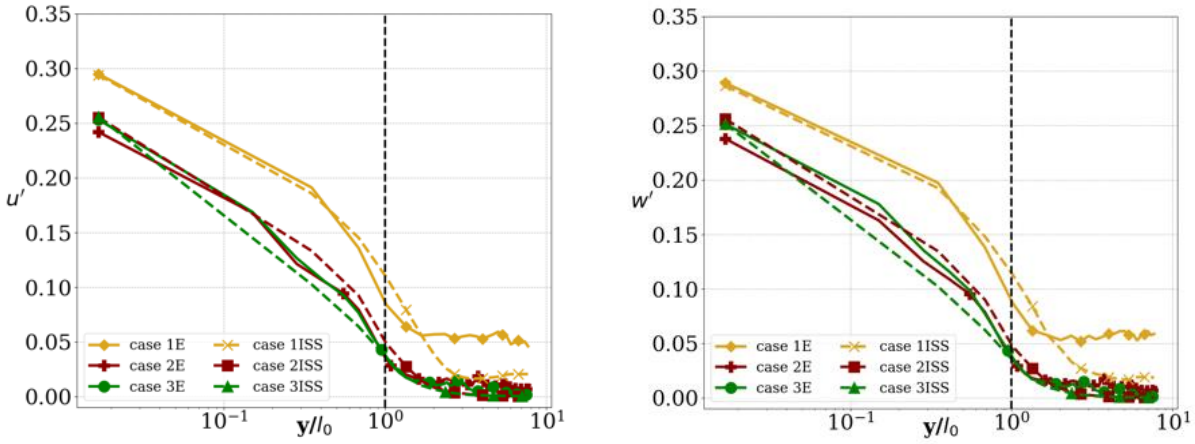

Figure 22: rms velocities fluctuations, u' and w' components at earth and ISS gravities.

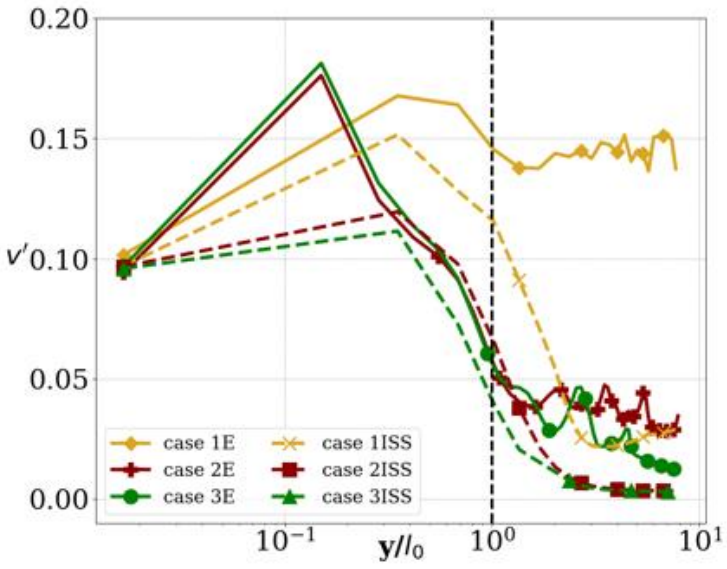

Figure 23: rms velocity fluctuations, v' component at earth and ISS gravities.

III. CONCLUSION

In this work, we investigate the effect of subcooling at earth gravity. We conducted same cases at ISS gravity. The main findings are the following: Earth gravity dynamics are governed by bubble growth, merging, and departure process; when the subcooling increases, departures decrease, and

bubble shrinking is observed. ISS gravity dynamics are governed by big bubbles that absorb the surrounding smaller bubbles. The growth process is more important at ISS gravity especially at low subcooling and tends to decrease with increasing the subcooling degree. An absence of departures was observed at ISS gravity for all subcooling cases using FC72 as working fluid. The difference in bubble dynamics between ISS gravity and earth gravity becomes negligible at high subcooling. The existence of an inflection point situated at $\Delta T_{sub} = 11℃$ for FC72 is also an important finding that was observed both at earth and ISS gravity. This indicates that subcooling does influence the heat flux and that it should be taken into consideration when using empirical correlations. Regarding the rms flow fluctuations, higher fluctuations were observed at low subcooling compared to high subcooling, clearly due to the big differences in bubble dynamics.

IV. AKNOWLEDEMENTS

The authors are grateful for the financial support by the National Aeronautics and Space Administration (NASA) Grant number: 80NSSC21K0470 monitored by Dr. David F. Chao. This research used NASA High Performance Computing Systems to run Direct numerical Simulations for 3D CFD cases. We thank NASA Advanced Supercomputing Division (NAS) for their generous allocation on Pleiades.

REFERENCES

1. Kim, J., Benton, J.F., Wisniewski, D., 2022. Pool boiling heat transfer on small. Heaters: effect of gravity and subcooling. International Journal of Heat and Mass Transfer 45, 3919-3932.
2. Rainey, K., You, S., 2001. Effects of heater size and orientation on pool boiling heat transfer from microporous coated surfaces. International Journal of Heat and Mass Transfer 44, 2589-2599.
3. Wang, C., Dhir, V., 1993. Effect of surface wettability on active nucleation site density during pool boiling of water on a vertical surface.
4. Jontz, P., Myers, J., 1960. The effect of dynamic surface tension on nucleate boiling coefficients. AIChE Journal 6, 34-38.
5. Mukherjee, A., Kandlikar, S.G., 2007. Numerical study of single bubbles with dynamic contact angle during nucleate pool boiling. International Journal of Heat and Mass Transfer 50, 127-138.
6. Son, G., Dhir, V.K., Ramanujapu, N., 1999. Dynamics and heat transfer associated with a single bubble during nucleate boiling on a horizontal surface.
7. Son, G., Dhir, V.K., 2008. Numerical simulation of nucleate boiling on a horizontal surface at high heat fluxes. International Journal of Heat and Mass Transfer 51, 2566-2582.
8. Van der Walt, S., Schönberger, J.L., Nunez-Iglesias, J., Boulogne, F., Warner, J.D., Yager, N., Gouillard, E., Yu, T., 2014. Scikit-image:image processing in python. PeerJ 2, e453.
9. Rohsenow, W.M., 1952. A method of correlating heat transfer data for surface boiling of liquids. Transactions of the American Society of Mechanical Engineers 74, 969-975.
10. Gaertner, R.F., 1965, Photographic study of nucleate pool boiling on a horizontal surface.
11. Stephan, K., Abdelsalam, M., 1980. Heat transfer correlations for natural convection boiling. International Journal of Heat and Mass Transfer 23, 73-87.

12. Linehard, J., 1963. A semi-rational nucleate boiling heat flux correlation. International Journal of Heat and Mass Transfer 6, 215-219.
13. Tien, C., 1962. A hydrodynamic model for nucleate pool boiling. International Journal of Heat and Mass Transfer 5, 533-540.
14. Hameed, M.S., Khan, A.R., Mahdi, A., 2013. Modelling a general equation for pool boiling heat transfer. Advances in Chemical Engineering and Science 2013.
15. Passos, J., Reinaldo, R., 2000. Analysis of pool boiling within smooth and grooved tubes. Experimental Thermal and Fluid Science 22, 35-44.
16. Monde, M., Katto, Y., 1978. Burnout in ahigh heat flux. Boiling system with an impinging jet. International Journal of Heat and Mass Transfer 21, 295-305.
17. Gunther, F.C., Kreith, F., 1950. Photographic study of bubble formation in heat transfer to subcooled water. Jet Propulsion Laboratory Progress Report, 1-29.
18. Ibrahim, E., Judd, R., 1985. An experimental investigation of the effect of subcooling on bubble growth and waiting time in nucleate boiling.
19. Goel, P., Nayak, A.K., Kulkarni, P.P., Joshi, J.B., 2017. Experimental study on bubble departure characteristics in subcooled nucleate pool boiling. International Journal of Multiphase Flow 89, 163-176.
20. Kim, J., Benton, J.F., 2002. Highly subcooled pool boiling heat transfer at various gravity levels. International Journal of Heat and Fluid Flow 23, 497-508.
21. Zhao,J.F., Wan., S.X.Liu,G., Hu, W.R., 2004b. Subcooled pool boiling in microgravity: results of drop tower testing, In: Proc. Of the 7th Drop Tower Days, Sept. 12-25, Bermen, Germany.
22. Mudawar, I., Anderson, T., 1990. Parametric investigation into the effects of pressure, subcooling, surface augmentation and choice of coolant on pool boiling in the design of cooling for high-power density electronic chips.
23. Youssoufi, S., Lentner, A., Riaz, A., Balaras, E., 2023. A Study Of Subcooled Pool Boiling Using Direct Numerical Simulations. Proceedings of the 4th International Conference on Fluid Flow and Thermal Science (ICFFTS'23), Lisbon, Portugal, December 07-09, 2023, DOI: 10.1159/icffts23.169.
24. Kang, M., Fedkiw, R.P, Liu, X.D, 2000. A boundary condition capturing method for multiphase incompressible flow. Journal of Scientific Computing 15, 323-360.
25. Dhruv, A., Balaras, E., Riaz, A., Kim, J., 2019. A formulation for high-fidelity simulations of pool boiling in low gravity. International Journal of Multiphase Flow 120, 103099.
26. Straub, J.: Boiling heat transfer and bubble dynamics in microgravity, Adv. Heat Transfer. 35, 57-172 (2001).
27. Di Marco, P.: Review of reduced gravity boiling heat transfer European research. J. Jpn. Microgravity Appl. 20, 252-263 (2003).
28. Kim, J.: Review of reduced gravity boiling heat transfer: US research. J. Jpn. Microgravity Appl. 20, 264-271 (2003).
29. Ohta, H.: Review of reduced gravity boiling heat transfer: Japanese research. J.Jpn. Microgravity Appl. 20, 272-285 (2003).
30. Zhao, Jian-fu. Two-phase flow and pool boiling heat transfer in microgravity. International Journal of Multiphase Flow 36.2 (2010): 135-143.
31. Zhao, J.F., Liu, G., Wan, S.X., Yan, N., 2008. Bubble dynamics in nucleate pool boiling on thin wires in microgravity. Microgravity Sci. Tech, 20(2), 81-89.